Analysis of photoconductive gain as it applies to single-photon detection

M. A. Rowe,[1,a)] G. M. Salley,[2] E. J. Gansen,[3] S. M. Etzel,[1] S. W. Nam,[1] and R. P. Mirin[1]
[1]*Optoelectronics Division, National Institute of Standards and Technology, Boulder, Colorado 80305, USA*
[2]*Department of Physics, Wofford College, Spartanburg, South Carolina 29303, USA*
[3]*Department of Physics, University of Wisconsin-La Crosse, La Crosse, Wisconsin 54601, USA*

(Received 4 December 2009; accepted 9 February 2010; published online 30 March 2010)

We detail a mathematical framework for photoconductive gain applied to the detection of single photons. Because photoconductive gain is derived from the ability to measure current change for an extended period, its magnitude is reduced as detection speed is increased. We theoretically show that high-speed detection is still possible as long as the noise spectrum of the device is $1/f$ in nature. Using signal analysis techniques, we develop tools to apply to device noise spectra to determine the performance of single-photon detectors that utilize photoconductive gain. We show that there is no speed penalty when one considers the signal-to-noise ratio for the fundamental $1/f$ noise typical of high electron mobility transistors. We outline a technique for quickly characterizing a detector's sensitivity and speed through purely electrical measurements of the device's noise spectra. Consequently, the performance of the detector can be determined and optimized without conducting optical measurements. Finally, we employ this analysis to a quantum dot, optically gated field-effect transistor and verify our results with optical measurements. © *2010 American Institute of Physics*. [doi:10.1063/1.3359684]

I. INTRODUCTION

Photoconductive gain provides an innovative means for detecting single photons.[1–9] In specialized high electron mobility transistors (HEMTs) photoexcited charge is amplified by the following mechanism: trapped charges produce a persistent change in the channel current of the transistor and this persistent change can be measured for an extended period. By using quantum dots (QDs) as charge traps, which can be controllably positioned within an engineered heterostructure, a device can be tailored for photon detection with high internal quantum efficiency and signal uniformity. Because photoconductive gain is applied independently and uniformly to each photon, well-resolved signals from different photon numbers have been demonstrated.[7] In addition, the photoconductive gain mechanism is always active and ready to detect; there is no intrinsic recovery period ("deadtime") after a photon event. More exotic device capabilities may also be possible due to the nondestructive mechanism associated with photoconductive gain. A photon is emitted for each trapped hole when the device is reset by injecting electrons into the QDs.[10–13] Consequently, these devices could serve as photon sources as well as photon detectors. In addition, the preservation of the spin of the detected photon by the photoexcited trapped charge could lead to spin coherent photodetectors or sources.[14–17] With these unique device capabilities, quantum information applications such as quantum memories or repeaters may be enabled.[18,19] We therefore require a more detailed understanding of the mechanics of photoconductive gain.

[a)]Electronic mail: mrowe@boulder.nist.gov.

II. DEVICE OPERATION

Here we provide a brief summary of the operation of a QD, optically gated, field-effect transistor (QDOGFET); more details can be found in Ref. 6. The QDOGFET is fabricated from a $GaAs/Al_{0.2}Ga_{0.8}As$ heterostructure that contains a layer of InGaAs QDs. The basic operation of the QDOGFET first requires the absorption of a photon, which creates an electron-hole pair in a dedicated absorption layer. Then the hole is efficiently directed with designed electric fields to the QD layer.[20] The hole is captured by a QD, where it partially screens the gate field, causing a change in the channel current that can persist for up to several seconds at 4 K. Given that the plane of QDs is geometrically well-defined, the detection response to each photon is uniform, resulting in a photon number-resolving detector. In addition, the detection mechanism is always active, regardless of prior photon events (until all of the QDs are filled), and thus the detector has no inherent deadtime. The result of every photon is stored as a persistent current change that lasts until the stored charge is erased. Because the underlying charge transport is very fast, evidenced by HEMT device frequencies exceeding 100 GHz,[21] the response time of the detector should be fundamentally very short.

A typical scenario of operation is illustrated in Fig. 1. Here, the detector is run in a continuous mode and illuminated with a train of 500 photon bursts from a highly attenuated laser at a repetition rate of 10 kHz. Each burst produces a persistent step in the detector output, resulting in a stair-step pattern for the entire burst train. The detector is sensitive to photons continuously until the QDs are full (several thousand photons detected for our device geometry), at which point it needs to be reset. To empty the QDs, we temporarily forward bias the gate. This fills the QDs with electrons that radiatively recombine with the holes and reset the device in

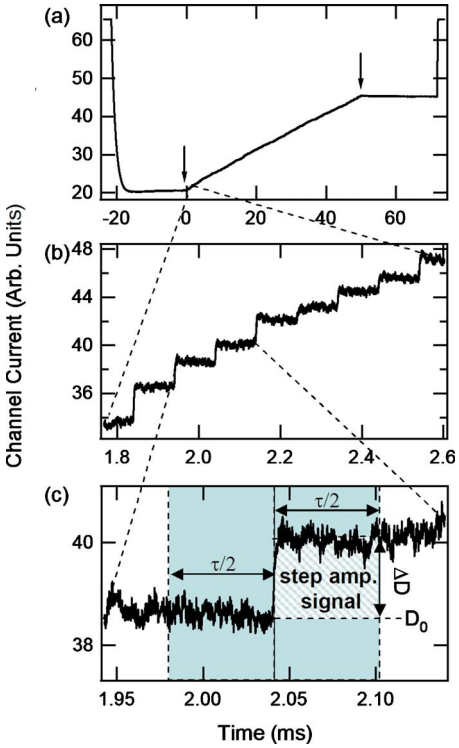

FIG. 1. (Color online) Time traces of the QDOGFET detector output responding to 500 photon bursts at 10 kHz. (a) The detector resets (beginning and end) plus the full illumination period (between arrows). (b) Magnifying the detail of the stair steps during illumination. (c) Detail of a single step, including parameters used in the detection analysis.

less than 1 μs. The electrical reset pulses are apparent in the output signal plotted in Fig. 1(a) as the spikes observed at the beginning and end of the trace. Once the device is reset, the output signal is constant until the burst train begins at the time indicated by the left arrow. The output then rises in discrete steps [magnified in Fig. 1(b)] until the burst sequence ends at the right arrow. The output is again constant until we apply the subsequent reset pulse at the end of the trace. For the data shown an average of 5 photons were detected per burst. The variation in step size results from the Poisson variation in the number of photons detected.

III. NOISE EQUATIONS FOR PHOTOCONDUCTIVE GAIN

To better illustrate the mechanics of photoconductive gain, we analyze a single step in the detector output signal. We note here that this analysis applies only when the timing of the light pulse is known. Figure 1(c) magnifies the detector output down to a single step and includes the relevant parameters used in the detection analysis. The output signal rises with the arrival of a photon burst and then is flat, following the time dependence, $D(t)=\Delta D u(t)+D_0$. Here ΔD is the step amplitude, $u(t)$ is the Heaviside function, D_0 is the step offset, and the arrival time of the photon pulse is at $t=0$. Although the step in the detector output persists for more than several seconds, we want to measure the step size in a much shorter period, τ. In Fig. 1(c), we show the time window (centered on the pulse arrival time) that we use in measuring the step amplitude. To use the full measurement period in reducing the impact of noise, we calculate the *step amplitude signal*, which is defined as the difference in the average areas under the detector output before and after the laser pulse. Formally, we apply an average difference filter, whose impulse response is

$$w(t) = -u(t+\tau/2)u(-t) + u(t)u(\tau/2-t), \tag{1}$$

to the output time sequence. According to standard signal processing, the step amplitude signal, S, is the peak value of the resulting time sequence, $S(t)=w^{*}D$, which occurs at $t=0$ and is

$$S = \int_{-\infty}^{\infty} D(t)w(t)dt = \Delta D\tau/2. \tag{2}$$

This step amplitude increases linearly with the measurement period as expected for photoconductive gain.

At first glance, it seems that averaging the detector output for a longer period τ should lead to a more accurate determination of the actual step size. However, this is not necessarily true because the optimal averaging period depends on the nature of the noise. The primary low frequency noise source for many HEMTs at 4 K has a $1/f$ noise spectral density[22] so we begin by calculating the noise result for this case. We will also show how this calculation can be interpreted in the presence of other noise spectra. We start by parametrizing the noise spectral density $N(f)$ of the detector output with a $1/f$ noise coefficient B as follows:

$$N(f) = B^2/f. \tag{3}$$

The application of the average difference filter weights the frequency components of this noise by

$$W(f) = (2/i\pi f)\sin^2(\pi f\tau/2), \tag{4}$$

which is the Fourier transform of $w(t)$. By applying the average difference filter to a series of uniform steps from a noisy detector, we determine a whole series of step amplitude signals. The distribution of these step amplitude signals has an average size, S, and standard deviation, σ, which can be calculated from the noise spectrum. This σ depends on the spectral content of the average difference filter and the noise spectral density as follows:

$$\sigma = \left[\int_0^{\infty} W^2(f)N(f)df\right]^{1/2}. \tag{5}$$

Evaluating the expression in Eq. (5) for our case gives

$$\sigma = B\tau\sqrt{\ln 2}. \tag{6}$$

This σ, which represents the step amplitude signal noise, increases linearly with τ. As a result, the signal-to-noise ratio (SNR) of the processed detector steps is independent of τ

$$\frac{S}{\sigma} = \frac{\Delta D}{2B\sqrt{\ln 2}}. \tag{7}$$

The detector can therefore be run arbitrarily fast without losing sensitivity as long as $1/f$ noise is the dominant noise mechanism. At some frequency the $1/f$ noise hits the thermal noise floor, and faster operation decreases sensitivity. How-

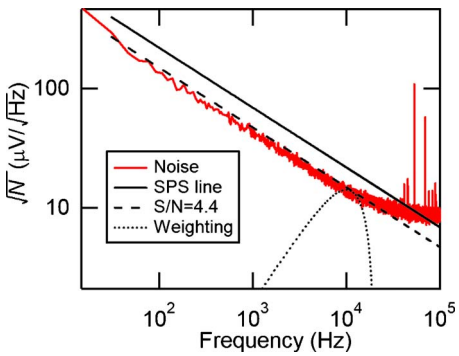

FIG. 2. (Color online) The square root of the noise spectral density for an amplified QDOGFET detector output. The SPS line is shown as a solid straight line. The line with SNR of 4.4 is shown as a dashed line. The weighting function for a measurement period of 100 μs is shown as a dotted curve.

ever, this noise floor corner frequency can be in the gigahertz range for HEMT devices.[23]

For a distribution of step amplitude signals, the S_1/σ ratio determines our ability to discriminate between one-photon and zero-photon events, where S_1 is the average step amplitude signal for a single photon. When $S_1/\sigma=3$, the zero-photon occurrences start to become resolved from the one-photon occurrences as explained below. Even in the non-ideal case, where there is additional broadening of the one-photon occurrences peak, the $S_1/\sigma=3$ criterion has a useful interpretation in terms of single-photon sensitivity. When $S_1/\sigma=3$ the discriminator level can be set at S_1, resulting in 50% of the nonzero occurrences being correctly designated with only 1% dark counts. Although it is somewhat arbitrary exactly what performance metrics are needed for single-photon sensitivity, we use the $S_1/\sigma=3$ criterion. The corresponding $1/f$ noise coefficient, $B(S_1/\sigma=3)$, is calculated from Eq. (7) and is

$$B(S_1/\sigma=3)=\frac{\Delta D_1}{6\sqrt{\ln 2}}\approx 0.2\Delta D_1. \tag{8}$$

Here ΔD_1 is the amplitude of the step caused by a single photon. Consequently, the noise spectral density that results in single-photon sensitivity (SPS) is given by

$$N_{\mathrm{SPS}}(f)=\frac{(\Delta D_1)^2}{36\ln 2f}. \tag{9}$$

This concept is easily generalized such that the noise spectral density that results in $S_1/\sigma=R$ is

$$N_R(f)=\frac{(\Delta D_1)^2}{4R^2\ln 2f}. \tag{10}$$

IV. EXPERIMENTAL VERIFICATION AND DISCUSSION

In our experiment the channel current is converted to voltage using a transimpedance amplifier with a transfer ratio of 3×10^5 Ω. For the experimental data that follow we discuss signals and noise in terms of this output voltage. Figure 2 shows the square root of the noise spectral density for the amplified QDOGFET detector output. The ΔD_1 is 11 mV for the operating conditions of Fig. 2. The SPS line from Eq. (9) is plotted as a solid line in Fig. 2 and indicates the maximum noise that allows single photon detection at a given frequency. The weighting function $W(f)$ from Eq. (4) with $\tau=100$ μs is also shown as a dotted curve. Because Eq. (5) is weighted by $W(f)$, which is peaked around the measurement frequency $f_m=1/\tau$, only the noise in the vicinity of f_m strongly influences σ. As a result, if the noise spectrum around f_m is below the SPS line the detector will be sensitive to single photons when run at the frequency f_m. The SPS line given by Eq. (9) therefore indicates which frequencies the detector will have SPS for a general noise spectrum. The application of this rule to noise spectra with highly resonant noise spikes or time correlated noise has limitations. In Fig. 2, the detector output noise starts to flatten out at about 20 kHz (due to the noise floor of a noisy exterior amplifier) and at about 50 kHz crosses the SPS line. In addition, the noise has spikes at higher frequencies, which are consistent with pick-up of external electromagnetic sources. Given this noise we expect SPS out to a measurement frequency of about 50 kHz. We can also predict the actual SNR at a desired measurement frequency by determining which $N_R(f)$ spectrum intersects the noise spectrum at the measurement frequency. For our example, with $\tau=100$ μs, we plot in Fig. 2 an $N_R(f)$ line (dashed line) with $R=4.4$. This line intersects the noise data at the frequency of interest, 10 kHz. As a result, we predict that the detector will be single-photon sensitive with $S_1/\sigma=4.4$ when illuminated by photons and measured at 10 kHz. We will show this sensitivity explicitly below.

In order to experimentally verify our model of single-photon sensitivity, we illuminated our QDOGFET detector with 5000 individual pulses from a highly attenuated laser, and we electrically reset the device between pulses. We analyzed the time traces of the detector output with various averaging periods τ. We applied the average difference filter from Eq. (1) to the time trace associated with each laser pulse and acquired 5000 step amplitude signals. We also acquired 5000 "dark step" amplitude signals by applying the average difference filter to the portions of the time trace where there was no laser pulse. In Fig. 3, we show the resulting distributions of the step amplitude signals for $\tau=100$ μs or $f_m=10$ kHz. Note that the actual detection frequency can be twice f_m or in this case, 20 kHz because consecutive measurement periods can overlap by half a period. The filled (open) circle histogram bins the step amplitude signals with (without) laser illumination. We determined the mean number of photon detected per pulse, λ, by fitting the fraction of zero-photon occurrences in the illuminated histogram. The probability of zero-photon occurrences is $P(0)=e^{-\lambda}$, giving us $\lambda=0.65$. By dividing the average step amplitude signal of the histogram in Fig. 3 by λ, we find that $\Delta D_1=11.1$ mV. Finally the step amplitude signal noise is found by fitting the nonilluminated histogram with a Gaussian. The resulting standard deviation was $\sigma=2.6$ mV. The result of our analysis of the photon data was therefore a SNR of 4.3. This value agrees well with our predicted value of 4.4, which was calculated using only the noise spectrum. With this signal-to-noise level we expect single-photon sensitivity. We verified this expectation by setting a discrimina-

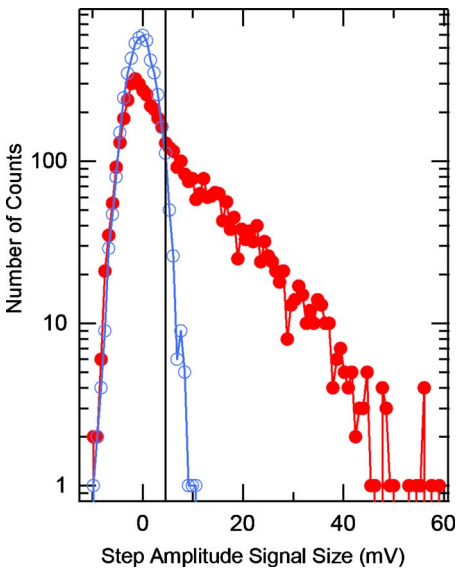

FIG. 3. (Color online) The histogram distribution of 5000 step amplitude signals for a measurement period of 100 μs. The filled (open) circle data resulted from illumination with a mean number of photons per pulse of 0.65 (0).

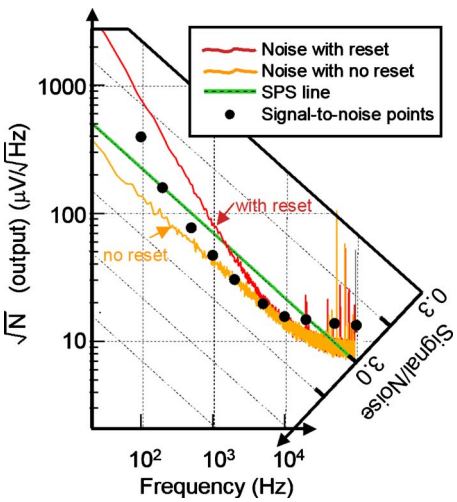

FIG. 4. (Color online) All of the noise data presented in this figure were taken with the same QDOGFET bias conditions. The filled circles are signal-to-noise points resulting from the analysis of photon data (as explained in the text) for a series of different measurement frequencies. They are graphed with respect to the diagonal axis on the right. The data marked "with reset" and "no reset" are the square root of the noise spectral densities for the labeled electrical reset condition. The left axis applies to these noise spectra. The solid diagonal line with signal-to-noise=3 is the SPS line from Eq. (9).

tor level, which is shown in Fig. 3 as a solid vertical line at 4.4 mV. Using this discriminator level we determined that with only 1.0% dark counts, 78% of the nonzero photon events are correctly designated. For the more stringent requirement of 0.1% dark counts, 64% of the nonzero photon events are correctly designated. The device used here did not include a metallic aperture that restricts absorption of photons to the uniform response area of the detector. As a result, the one-photon occurrences peak is quite wide. An apertured device should have a similar SNR. Its improved signal uniformity should not only give it number-resolving capability but improve the fraction of correctly designated nonzero photon events.

With the same photon data, we analyzed the SNR for a series of different measurement frequencies to show the degree of agreement with the noise spectrum predictions at a variety of measurement frequencies. The filled circles in Fig. 4 are the signal-to-noise points resulting from this analysis of the photon data. These are graphed as a function of f_m with respect to the axis on the right, where the lines of constant signal-to-noise are diagonals. The diagonal with SNR=3 is highlighted with a solid line to emphasize that it is the SPS level. In addition, it is the SPS line of Eq. (9) and therefore fixes the scaling of the left or noise density axis. The SNR points associated with the measurement frequencies of 200 Hz–20 kHz (detection frequencies of 400 Hz–40 kHz) lie at or below this SPS line and are therefore single-photon sensitive. In Fig. 4, the square root of two noise spectral densities, graphed with respect to the left axis, overlie the SNR data. As discussed above, spectral points that lie on the $N_R(f)$ spectrum of Eq. (10) (lines for the log/log graph) have a SNR of R. Graphing the data this way shows that the signal-to-noise points lie on top of the noise spectra. The "with reset" ("no reset") spectrum was taken with the same operating conditions as the photon data, including (not including) the electrical reset. The "with reset" spectrum has a low-frequency $1/f^2$ dependency (for the noise spectral density), the signature of time-coherent steps. We believe that the reset populates defect traps, which then decay randomly, giving this $1/f^2$ signature. Because this reset noise source is time coherent, the experimental SNRs are better than the "with reset" spectrum predicts. They are between the predictions of the "no reset" and "with reset" spectra, and above 1 kHz the reset noise contribution is minimal. Thus the "no reset" spectrum predicts the best achievable noise level. In principle, the reset strength/wait period can be adjusted to get to this level if needed. However, since higher detection frequencies are desired, the reset noise is not a problem. At intermediate frequencies the SNR points do lie on top of the noise spectra, as predicted. At higher frequencies, where there are noticeable pick-up noise spikes, the SNR points are above the baseline of the spectra, indicating that the pick-up noise is significant. Again, the baseline provides the achievable noise level if this pick-up noise is eliminated. The analysis outlined here can be used as a predictive tool to understand how improvements such as eliminating pick-up or improved amplifier design can translate to photon detection improvements.

To compare the noise of a device in different configurations, we normalize the square root of the noise spectral density by dividing it by the single photon step size ΔD_1. Similarly, a normalized SPS line is found by dividing the SPS line formula [Eq. (9)] by $(\Delta D_1)^2$. Multiple normalized noise spectra can then be directly compared, and the normalized SPS line applies to all of them. ΔD_1 can be experimentally found, as above, by illuminating the device with photons. This is not required because we have shown previously that the theoretical value of ΔD_1 and the experimental value of ΔD_1 agree quite well.[6] By using the theoretical value of ΔD_1 a device can be rapidly characterized without measuring ΔD_1 directly. In Ref. 6, we showed that the effective change in the gate voltage, $\Delta V_{\text{gate}}(1)$, due to one photon is

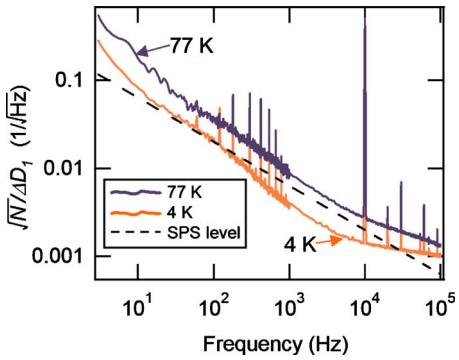

FIG. 5. (Color online) Normalized noise spectra for the same QDOGFET operated at 4 and 77 K (as marked). The dashed line is the normalized SPS line and the spike at 10 kHz is the result of the calibrating gate modulation.

$$\Delta V_{\text{gate}}(1) = \frac{eW}{\varepsilon' A}, \tag{11}$$

where e is the elementary charge, W is an epitaxial layer thickness, ε' is the electric permittivity of the material, and A is the active area of the detector.[6,24] Thus, to find the value of ΔD_1, we modulate the gate with an amplitude that is a known multiple of $\Delta V_{\text{gate}}(1)$, and then the detector output amplitude is the same multiple of ΔD_1. As an example of this technique, Fig. 5 shows normalized noise spectra for the same device operated at 4 and 77 K (as marked). The dashed line is the normalized SPS line and the spike at 10 kHz is the result of the calibrating gate modulation. Both spectra were taken with bias parameters that maximized the device transconductance. The additional noise spikes (100–1000 Hz) present in these spectra (and not the previous spectra) are an artifact of the grounding of the signal generator used to modulate the gate voltage. These 60 Hz harmonics from ground loops are not present when the detector is run in photon detection mode and thus may be disregarded. The noise spectra also exhibit features (broad bumps) at about 100 Hz and 10 kHz that are consistent with generation-recombination in the heterostructure. Interestingly, these features do not increase in size with temperature, while the fundamental $1/f$ noise does. Although the step signals are still persistent at 77 K, SPS is not achievable, due to excess noise. The normalized noise spectrum lies above the normalized SPS line for all of the frequencies. Mapping the temperature dependencies of the different noise components will determine whether operation at 77 K or higher is possible. Relating single photon detector performance to a noise spectrum enables us to understand and predict device performance over a wide range of operating conditions.

V. CONCLUSION

We have presented a mathematical framework for understanding single photon detectors that rely on photoconductive gain. Photoconductive gain does not fundamentally limit the detection speed as long as the associated noise spectrum has a $1/f$ dependency. If this is the case the detector can be operated arbitrarily fast with the same photon detection sensitivity as at slower speeds. Although here we showed this result for a specific average difference filter, which we believe has close to optimal sensitivity, this finding applies generally to all filter operations. Photon sensitivity decreases as the detection frequency approaches the noise floor, corner frequency, but this speed-limiting noise-floor corner frequency can be in the gigahertz range for HEMTs. We have directly related the noise spectrum to a detector's performance and verified these relationships with QDOGFET detectors. As a specific example, we verified the predicted SPS for an illuminated QDOGFET for a measurement frequency of 10 kHz. A wide range of variational studies (detector area, temperature, biases, epitaxial composition, and Ohmic contact chemistry) are now possible without illuminating the detector, allowing the quick optimization of a detector's performance. These tools will also be useful to further pursue the root causes of different noise sources and thus minimize the errant noise components. In addition, by isolating just the fundamental noise of a device, predictions of its inherent performance capabilities can be made.

[1] A. J. Shields, M. P. O'Sullivan, I. Farrer, D. A. Ritchie, R. A. Hogg, M. L. Leadbeater, C. E. Norman, and M. Pepper, Appl. Phys. Lett. **76**, 3673 (2000).
[2] H. Kosaka, D. S. Rao, H. D. Robinson, P. Bandaru, T. Sakamoto, and E. Yablonovitch, Phys. Rev. B **65**, 201307(R) (2002).
[3] H. Kosaka, D. S. Rao, H. D. Robinson, P. Bandaru, K. Makita, and E. Yablonovitch, Phys. Rev. B **67**, 045104 (2003).
[4] B. E. Kardynal, A. J. Shields, N. S. Beattie, I. Farrer, K. Cooper, and D. A. Ritchie, Appl. Phys. Lett. **84**, 419 (2004).
[5] J. D. Kiely and Y.-T. Hsia, J. Appl. Phys. **98**, 114501 (2005).
[6] M. A. Rowe, E. J. Gansen, M. Greene, R. H. Hadfield, T. E. Harvey, M. Y. Su, S. W. Nam, and R. P. Mirin, Appl. Phys. Lett. **89**, 253505 (2006).
[7] E. J. Gansen, M. A. Rowe, M. B. Greene, D. Rosenberg, T. E. Harvey, M. Y. Su, R. H. Hadfield, S. W. Nam, and R. P. Mirin, Nat. Photonics **1**, 585 (2007).
[8] B. E. Kardynal, S. S. Hees, A. J. Shields, C. Nicoll, I. Farrer, and D. A. Ritchie, Appl. Phys. Lett. **90**, 181114 (2007).
[9] H. W. Li, B. E. Kardynal, P. See, A. J. Shields, P. Simmonds, H. E. Beere, and D. A. Ritchie, Appl. Phys. Lett. **91**, 073516 (2007).
[10] T. Lundstrom, W. Schoenfeld, H. Lee, and P. M. Petroff, Science **286**, 2312 (1999).
[11] H. Pettersson, L. Baath, N. Carlsson, W. Seifert, and L. Samuelson, Appl. Phys. Lett. **79**, 78 (2001).
[12] M. Kroutvar, Y. Ducommun, J. J. Finley, M. Bichler, G. Abstreiter, and A. Zrenner, Appl. Phys. Lett. **83**, 443 (2003).
[13] E. J. Gansen, M. A. Rowe, M. B. Greene, D. Rosenberg, T. E. Harvey, M. Y. Su, R. H. Hadfield, S. W. Nam, and R. P. Mirin, IEEE J. Sel. Top. Quantum Electron. **13**, 967 (2007).
[14] R. Vrijen and E. Yablonovitch, Physica E (Amsterdam) **10**, 569 (2001).
[15] M. Kroutvar, Y. Ducommun, D. Heiss, M. Bichler, D. Schuh, G. Abstreiter, and J. J. Finley, Nature (London) **432**, 81 (2004).
[16] H. Kosaka, H. Shigyou, Y. Mitsumori, Y. Rikitake, H. Imamura, T. Kutsuwa, K. Arai, and K. Edamatsu, Phys. Rev. Lett. **100**, 096602 (2008).
[17] H. Kosaka, T. Inagaki, Y. Rikitake, H. Imamura, Y. Mitsumori, and K. Edamatsu, Nature (London) **457**, 702 (2009).
[18] E. Yablonovitch, H. W. Jiang, H. Kosaka, H. D. Robinson, D. S. Rao, and T. Szkopek, Proc. IEEE **91**, 761 (2003).
[19] H.-J. Briegel, W. Dür, J. I. Cirac, and P. Zoller, Phys. Rev. Lett. **81**, 5932 (1998).
[20] M. A. Rowe, E. J. Gansen, M. B. Greene, D. Rosenberg, T. E. Harvey, M. Y. Su, R. H. Hadfield, S. W. Nam, and R. P. Mirin, J. Vac. Sci. Technol. B **26**, 1174 (2008).
[21] C. Y. Chang and F. Kai, *GaAs High-Speed Devices* (Wiley, New York, 1994).
[22] F. Ali and A. Gupta, *HEMTS and HBTS Devices: Devices, Fabrication and Circuits* (Artech House, Boston, 1991).
[23] S.-M. J. Liu, S. T. Fu, M. B. Das, K.-H. G. Duh, P. C. Chao, P. M. Smith, and J. M. Ballingall, Tech. Dig. - Int. Electron Devices Meet. **1987**, 414.
[24] G. Yusa and H. Sakaki, Electron. Lett. **32**, 491 (1996).